Łukasz MACIURA[1], Wojciech ROSA[2], Dariusz WÓJCIK[1], Tomasz Rymarczyk[13], Michał MAJ[13], Edward KOZŁOWSKI[13]

Netrix S.A., Research & Development Centre, Lublin, Poland (1),
Lublin University of Technology, Lublin, Poland (2),
University of Economics and Innovation in Lublin, Poland (3)

doi:10.15199/48.2022.05.31

3D lung segmentation of the CT series based on 2D Chan-Vese

Abstract*. This paper presents a new 3D segmentation algorithm for lung segmentation tasks on CT series. The algorithm consists of a 2D stage (for each slice) which is performed parallelly and 3D postprocessing after merging to 3D. The 2D stage consists of 2D preprocessing, Chan - Vese segmentation, and 2D postprocessing. This algorithm was tested on the set of 60 CT series containing labelled data enable to its assessment. The results of the algorithm are close to deep learning approaches. This algorithm will be an element of a commercial expert system for medical applications where some patient assessment will be necessary based on segmented human organs.*

Streszczenie. *Ten artykuł prezentuje nowy algorytm segmentacji 3D do zadań segmentacji płuc na seriach z tomografii komputerowej. Ten algorytm składa się z etapu 2D (dla każdego przekroju) który jest wykonywany równolegle i post-processingu 3D po scaleniu wyników do 3D. Etap 2D składa się z pre-processingu 2D, segmentacji Chan – Vese I post-processingu 2D. Algorytm był przetestowany na zbiorze 60 serii obtazów z tomografii komputerowej zawierających zaetykietowane dane co umożliwiło jego ocenę. Wyniki algorytmu są przybliżonej dokładności do rozwiązań deep learning. Algorytm ten będzie elementem komercyjnego system ekspertowego do zastosowań medycznych, gdzie niezbędna będzie ocena pacienta bazując na segmentowanych organach człowieka. (****Nowy algorytm segmentacji 3D płuc na seriach z tomografii komputerowej bazujący na Chan – Vese 2D****)*

Keywords: CT segmentation, medical imaging, Chan – Vese segmentation.
Słowa kluczowe: segmentacja obrazów z tomografii komputerowej, obrazowanie medyczne, segmentacja Chan – Vese.

Introduction

The CT image segmentation tasks are handy in medical expert systems nowadays. Below presented lungs segmentation algorithm was created as a part of a medical expert system needing lungs volume calculation for the patient based on CT DICOM images. Many segmentation algorithms can be used in medical imaging. One of the most popular algorithms used in medical image segmentation is the active contour algorithm [1]. The other image segmentation algorithms are also helpful: level set algorithm [2], [3], random walker algorithm [5] and others.

In the paper, [4] the segmentation of lungs in X-ray image using a level set method is presented. In the MatLab tutorial [7], the lungs segmentation using Chan - Vese 3D algorithm is presented. Some elements of the preprocessing stage in the created lungs segmentation algorithm are similar

Nowadays, the best accuracy algorithms use deep learning segmentation [9], but as shown in this paper, using traditional image segmentation algorithms, we can achieve similar accuracy. During the creation of the CT segmentation algorithm, a special kind of active contour algorithm but without edges: the Chan - Vese algorithm [6] was used. The medical image segmentation algorithms could be assessed and compared to each other using many measures [11] as DICE, Jaccard, sensitivity, specificity, fallout, FNR, precision, FMS, accuracy measures but the most commonly used measure to compare the medical image segmentation algorithm is a DICE coefficient.

Chan – Vese algorithm

There are many methods for solving numerial problems [14-23]. The Chan - Vese algorithm [6] is a kind of active contour algorithm [1] but without edges. This algorithm uses a new active contours model to detect objects in a given image based on: curve evolution, Mumford-Shah functional model for segmentation and level sets [2].

Created CT image segmentation algorithm

A. Preprocessing in 2D

The images from CT scans are at the beginning converted to Hounsfield Units (HU). The original voxels from the DICOM series are converted to HU using the following formula:

$$V_{HU} = V * m + b \tag{1}$$

where *m* is *RescaleSlope* tag and *b* is *RescaleIntercept* tag read from DICOM file.

The Hounsfield Units must have comparable voxel values for the same human tissues for multiple DICOM series. After reading of series with HU conversion, the proper 2D preprocessing could be performed for each slice. It consists of the following steps:

1) Voxels conversion in order to improve contrast in an image by the following thresholding:

$$v(x,y)' = \begin{cases} v(x,y), & if\ v(x,y) \geq C_{th} \\ C_{th}, & otherwise \end{cases} \tag{2}$$

where v and v' are old and new voxels values and C_{th} is the contrast threshold. The C_{th} threshold has another value for male and female patients where the sex of the patient is extracted from the DICOM file. This converted slice will be used as the first input to the Chan - Vese algorithm

2) Creation of initial binary image of lungs (second input to Chan - Vese algorithm)
   a. Simple thresholding in order to obtain human tissues (not containing area inside lungs and air outside the body):

$$B(x,y) = \begin{cases} 1, & if\ v(x,y) > S_{th} \\ 2, & otherwise \end{cases} \tag{3}$$

   b. Inversion of all voxels in the binary image:

$$B(x,y)_{inv} = 1 - B(x,y)$$

   c. Finally generation of a mask by the binary erosion calculation on the binary image from the previous step:

$$B_{mask} = B_{inv} \ominus S_e \tag{4}$$

where E is the binary erosion operation, and Se is the 2D structural element in disk shape and radius equal 3

B. Proper Chan – Vese segmentation

After the 2D preprocessing stage for the current processed stage, the proper Chan - Vese segmentation stage is performed. The used Chan - Vese algorithm implementation comes from the scikit - image Python library. The algorithm settings were tuned after multiple tuning stages, and except for the converted image and binary mask, the other parameters have values as in Table I.

Table I. Chan – Vese algorithm settings

id	parameter	value
1	μ	0.25
2	λ_1	1.0
3	λ_2	1.0
4	*tol*	0.005
5	max_{it}	100
6	δ_t	0.2
7	ext_{out}	false

2D postprocessing after segmentation

Directly after segmentation, there is a 2D postprocessing stage. This postprocessing stage consist of 2 substages:

1) Background objects removal from binary Chan - Vese output. During this substage, the objects in the binary image (Chan - Vese output) are labelled, and after collection, the objects labels near the image borders these objects are removed from the image. It is done because Chan - Vese is sometimes wrong, and other human tissues surround lungs, so there are not connected with the border.
2) If the result is still wrong (the result object is more than 5 times bigger than the binary mask object), the empty image is returned.
3) Binary closing operation of binary image from previous step:

$$B_{out} = B_{prev} \bullet S_e \tag{5}$$

where B_{out} is the final result of the algorithm for one slice, B_{prev} is the binary result from the previous stage and S_e is a structural element with disk shape kernel and different kernel rays for male and female patients.

C. Final 3D postprocessing

After processing of images for all slices (this operation is performed parallelly) and joining the images into one 3D binary image, the final 3D postprocessing stage is performed.

The final 3D postprocessing algorithm has the following form:

1) Creation of a 3D binary image from particular binary results for each slice
2) Calculation of mass centre (mc) of all 3D binary objects (lungs with noise) and checking the shift of mass centre in the x-axis:

$$|256 - mc_x| > Sh_t \tag{6}$$

If the shift is greater than the shift threshold (Sh_t) then there is detected that one lung is almost completely removed and the Sz_t threshold for the next step should be smaller; otherwise, it should be more extensive.

3) Delete objects not connected with lungs (which have a size smaller than the Sz_t threshold designated in the previous step)
4) Trachea removement (this algorithm will be explained separately)
5) Binary erosion performed on 3D binary image B3Dtr obtained in the previous step (after trachea movement)

$$B3D_e = B3D_{tr} \ominus S_{e3D} \tag{7}$$

where $S_{e3D}$is a 3D structural element in the shape of a ball with a radius equal 2

6) Very small objects in each slice movement (in order to finally disconnect objects) - for each slice, the small objects (which has size lower than Sz_{t2}) voxels are removed.
7) Removement of objects not connected with lungs (which have a size smaller than Sz_t threshold designated in the first step) once again obtaining $B3D_r$ image
8) Binary dilation:

$$B3D_d = B3D_r \oplus S_{e3D} \tag{8}$$

9) Binary closing:

$$B3D_c = B3D_d \bullet S_{e3D} \tag{9}$$

Notice that steps 5 and 8 can be considered as extended opening operations with objects separation and movement of wrong objects between erosion and dilation. Considering the above opening (steps 5 and 8) and closing (step 9) operations create together OC (opening-closing) morphology filter. OC binary morphology filter is defined as:

$$OC(B, se) = \big((B \circ se) \bullet se\big) \tag{10}$$

where B is a binary image and *se* is a structural element. The mentioned earlier operations in the algorithm could be considered as extended OC filtration, which has 2 roles: final smoothing of the 3D object and helps in the removal of elements not belonging to the lungs.

D. Trachea removal step

The trachea removal step (step no. 4) in the 3D postprocessing stage described in the above subsection. The trachea is often segmented with lungs, and it should be removed. The trachea removal algorithm relies on trachea tracking in 2D slice by slice and removal of found trachea from slices using binary XOR operation.

The trachea tracking and removal algorithm process all slices starting from the last slice of the segmentation image (from the top of the human body) and ending in the first slice. For each not empty slice, the following operations are performed:

1. The objects smaller than Sz_{t2} are removed
2. Creation of labelled image L (with labelled objects) from a slice Sz_{t2}
3. Obtaining the number of objects by getting maximal value
4. Calculation of centres of objects
5. Center of trachea extraction (c): In the case when there is one object only, then the centre of trachea is the centre of this object; otherwise, the centre of trachea is the centre of the object nearest to the centre of trachea position from previous slice or centre of the image wherein the previous slice trachea was not found
6. Trachea object extraction B_{tr} using c
7. Calculation of the trachea size S_{tr} (sum of trachea object pixels)
8. In the case when in the current slice and previous slice the trachea object was detected, then the distance d between both trachea objects centres is calculated
9. When the distance d is more significant than the distance threshold $d_{th}$and simultaneously size of the object detected as trachea from the previous

slice is greater than the object detected as trachea in the current slice, then the loop is finished.

10. Finally (if the loop was not finished in the previous step), the trachea removement procedure is performed using XOR operation between slice with segmentation and slice with extracted trachea object. The result is saved in the current segmentation slice.

The trachea tracking and removal algorithm is presented in the following pseudocode:

```
trachea_end ← false
last_p ← none
for i ← (n-1) to 0 do
   calculate slice voxels sum: s ← ∑_{v∈Sl_i} v
   if s>0 then
       small objects removement with size smaller than Sz_t2
       creation labelled image L from slice Sl_i
       nobjects ← max(L)
       centers ← MassCenters(L)
       if nobjects = 1 then
             p ← center s_0
       end
       else
             if last_pos = none then
                   p ← NearestToCenter(centers)
             end
             else
                   p ← NearestToObj(last_p,centers)
             end
       end
       trachea only object extraction B_tr using p
       S_tr ← size(B_tr)
       if last_p != none then
             dist ← Dist(p,last_p)
             if dist > 20 and size(Sl_{i-1}) > S_tr then
                   trachea_end ← true
             end
       end
       last_p ← p
       if trachea_end then
             break
       end
       else
             BW_out ← XOR(slice, B_tr)
             Sl_i ← BW_out
       end
end
```

where:
S_{li} - is i - th slice, size - is the function to calculate the sum of all non-zero elements in the image, max - is the function to calculate maximal element of the matrix,
MassCenters - is the function to calculate mass centres of objects in the labelled image,
NearestToCenter - is the function to choose one position from a list of positions nearest to the centre of the image,
NearestToObject - is the function to choose one position from a list of positions nearest to a given position,
Dist - is the function to calculate distance between points,
XOR - is the function to calculate *XOR* operation between corresponding voxels from input images.

Tuning of parameters on male and female patients separately

The tuning of some parameters of the algorithm was performed for male and female patients separately. Thanks to it the better results were achieved. Several parameters were tried to tune this way, but in two cases, the separately tuned parameters gave the better accuracy: contract threshold C_{th} in 2D preprocessing stage and structural element S_e of binary closing operation in the 2D postprocessing stage. For instance, we can see the optimal values of C_{th} the threshold for male and female patients obtained during the tuning process performed on the training dataset (II).

Table II. Contrast threshold C_{th} tuning for male and female patients

Id	HU_{thr}	DICE (female)	DICE (male)
1	-320	96.68	-
2	-330	96.69	-
3	-335	96.69	-
4	-340	96.69	-
5	-350	96.68	96.36
6	-360	96.67	96.37
7	-370	-	96.5
8	-375	-	96.49
9	-380	-	96.49

Since all parameters were not tuned for male and female patients separately, there is possible to obtain more parameters that could have other optimal values for male and female patients separately.

Results of algorithm

The result of the algorithm is in the form of a 3D binary image for one series. To visually show the result, the mesh should be created. We can see the sample output by using Marching Cubes algorithm [12], Figure 1.
The result binary images are compared with labelled images by using the DICE coefficient [11] (most popular measure), which could be defined as:

$$DICE = \frac{2\left|S_g^1 \cap S_t^1\right|}{\left|S_g^1\right| + \left|S_t^1\right|} = \frac{2TP}{2TP + FP + FN} \quad (11)$$

where: S_g^1 - is a set of voxel coordinates in result 3D image with a positive value, S_t^1 A set of voxel coordinates in labelled images with a positive value, TP, FP, FN - are numbers of true positives, false positives, and false negatives, respectively.

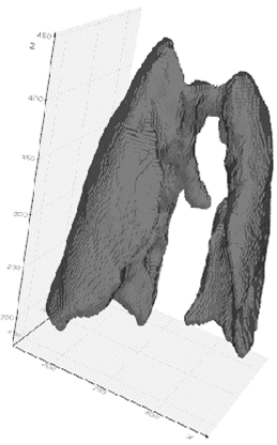

Fig. 1. 3D visualization of sample result of algorithm.

The method was evaluated on the 2017 AAPM Thoracic Auto-segmentation Challenge [13]. The dataset used for algorithm development and testing contained 60 series (one series per patient) and was divided by the organizers to the training dataset (containing 36 series) and test dataset (containing 24 series).
Finally, the DICE average of 96.99 was achieved on the training dataset, while the DICE average of 96.68 was achieved on the test dataset. These results are close to the deep learning approach [9], [10].

Conclusion

In this paper, a new lung segmentation algorithm was presented. This algorithm uses the Chan - Vese 2D segmentation algorithm with several own preprocessing and postprocessing stages, creating an original scientific solution. It has a high accuracy close to deep learning solutions. Since there are still some possibilities for further improvement of the algorithm, the accuracy could be better and could even exceed the accuracy of deep learning solutions. This algorithm will be an element of a commercial expert system for medical applications where some patient assessment will be necessary based on segmented human organs.

Authors:
dr inż. Łukasz Maciura E-mail: lukasz.maciura@netrix.com.pl,
dr inż. Dariusz Wójcik E-mail: dariusz.wojcik@netrix.com.pl,
Netrix S.A., Research & Development Centre, Lublin, Poland
Mgr inż. Wojciech Rosa E-mail: wrosa@pollub.pl
Dr hab. Edward Kozłowski
Lublin University of Technology Lublin, Poland
dr hab. inż. Tomasz Rymarczyk,
mgr inż. Michał Maj
Netrix S.A, Reseach & Development Centre, Lublin, Poland
University of Economics and Innovation in Lublin, Poland

REFERENCES

[1] M. Kass, A. Witkin, D. Terzopoulos, Snakes: Active contour models, International Journal of Computer Vision, 1988
[2] S. Osher, R. Fedkiw, Level Set Methods and Dynamic Implicit Surfaces Springer, New York, 2003
[3] X. Jiand, R. Zhang, S. Nie, Image Segmentation Based on Level Set Method 2012 International Conference on Medical Physics and Biomedical Engineering
[4] P. Annangi, S. R. Thiruvenkadam, X. Sun, L. Mao, A region based active contour method for x-ray lung segmentation using prior shape and low level features IEEE International Symposium on Biomedical Imaging: from nano to macro. IEEE International Symposium on Biomedical Imaging, Jan. 2010
[5] Leo Grady, Random walks for image segmentation, IEEE Trans. Pattern Anal. Mach. Intell. 2006
[6] T. F. Chan, L. A. Vese, Active Contours Without Edges, IEEE TRANSACTIONS ON IMAGE PROCESSING, VOL. 10, NO. 2, FEBRUARY 2001
[7] Segment Lungs from 3-D Chest Scan,https://www.mathworks.com/help/images/segment-lungs-from-3-dchest-mri-data.html
[8] J. Larrey-Ruiz et. al., Automatic image segmentation of the heart from CT scans EURASIP Journal on Image and Video Processing, 201
[9] Y. Lei et al., Deep Learning in Multi-organ Segmentation arxiv.org, 2020
[10] X. Dong et al., Automatic multiorgan segmentation in thorax CT images using U-net-GAN Medical Physics, 46(5), 2157–2168. https://doi.org/10.1002/mp.13458
[11] A. Aziz Taha, A. Hanbury, Metrics for evaluating 3D medical image segmentation: analysis, selection, and tool, BMC Medical Imaging, https://www.ncbi.nlm.nih.gov/pmc/articles/PMC4533825/ [12] W. Lorensen, William, H. E. Cline, Marching Cubes: A High Resolution 3D Surface Construction Algorithm, Computer Graphics (SIGGRAPH 87 Proceedings) 21(4) July 1987, p. 163-170). DOI:10.1145/37401.37422
[13] 2017 AAPM Thoracic Auto-segmentation Challenge, http://aapmchallenges.cloudapp.net/competitions/3, accessed 2020.10.12
[14] Filipowicz, SF and Rymarczyk, The Shape Reconstruction of Unknown Objects for Inverse Problems Przeglad Elektrotechniczny, 88 (3A), 55-57,2012.
[15] Rymarczyk T.: Characterization of the shape of unknown objects by inverse numerical methods, Przeglad Elektrotechniczny, 88(7B), 138-140,2012.
[16] Rymarczyk, T Using electrical impedance tomography to monitoring flood banks 16th International Symposium on Applied Electromagnetics and Mechanics (ISEM),International journal of applied electromagnetics and mechanics 45, 489-494,2014.
[17] Duraj, A.; Korzeniewska, E.; Krawczyk, A. Classification algorithms to identify changes in resistance. Przegląd Elektrotechniczny 2015, 1, 82–84.
[18] Krawczyk, A.; Korzeniewska, E. Magnetophosphenes–history and contemporary implications. Przegląd Elektrotechniczny 2018, 1, 63–66.
[19] Mosorov, V ; Rybak, G ; Sankowski, D, Plug Regime Flow Velocity Measurement Problem Based on Correlability Notion and Twin Plane Electrical Capacitance Tomography: Use Case, Sensors Volume: 21 Issue: 6 Article Number: 2189 DOI: 10.3390/s21062189, 2021.
[20] Koulountzios P., Rymarczyk T., Soleimani M., A quantitative ultrasonic travel-time tomography system for investigation of liquid compounds elaborations in industrial processes, Sensors, 19(23), 5117, 2019.
[21] Kłosowski G., Rymarczyk T., Kania K., Świć A., Cieplak T., Maintenance of industrial reactors based on deep learning driven ultrasound tomography, Eksploatacja i Niezawodnosc – Maintenance and Reliability; 22(1), 138–147, 2020.
[22] Kłosowski G., Rymarczyk T., Cieplak T., Niderla K., Skowron Ł., Quality Assessment of the Neural Algorithms on the Example of EIT-UST Hybrid Tomography, Sensors, 20(11), 3324, 2020.
[23] Łukiański, M., & Wajman, R. (2020). The diagnostic of two-phase separation process using digital image segmentation algorithms. Informatyka, Automatyka, Pomiary W Gospodarce I Ochronie Środowiska, 10(3), 5-8.